Materials Transactions, Vol. 49, No. 11 (2008) pp. 2559 to 2565
Special Issue on Advances in Computational Materials Science and Engineering V

Multi-Phase-Field Model to Simulate Microstructure Evolutions during Dynamic Recrystallization

Tomohiro Takaki[1], Tomoyuki Hirouchi[2,*], Yousuke Hisakuni[2,*], Akinori Yamanaka[3,*] and Yoshihiro Tomita[2]

[1]*Graduate School of Science and Technology, Kyoto Institute of Technology, Kyoto 606-8585, Japan*
[2]*Graduate School of Engineering, Kobe University, Kobe 657-8501, Japan*
[3]*Graduate School of Science and Technology, Kobe University, Kobe 657-8501, Japan*

A numerical model to simulate microstructure evolution and macroscopic mechanical behavior during hot working was developed. In this model, we employed a multi-phase-field model to simulate the growth of dynamically recrystallized grains with high accuracy and the Kocks-Meching model to calculate the evolution of dislocation density due to plastic deformation and dynamic recovery. Furthermore, an efficient computational algorithm was introduced to perform the multi-phase-field simulation efficiently. The accuracy of the developed model was confirmed by comparing the migration rate of grain boundaries with the theoretical value. Also, the numerical results for a polycrystalline material are compared with those obtained from a cellular automaton simulation. Furthermore, the effects of the initial grain size, grain boundary mobility and nucleation rate on the dynamic recrystallization behavior were investigated using the developed model.
[doi:10.2320/matertrans.MB200805]

(Received April 28, 2008; Accepted June 6, 2008; Published July 16, 2008)

Keywords: *phase-field method, dynamic recrystallization, microstructure, mechanical behavior, numerical scheme*

1. Introduction

During the hot working of metallic materials, hardening caused by the accumulation of dislocations and softening due to dynamic recovery (DRV) and dynamic recrystallization (DRX) occur simultaneously.[1)] In particular, for metals with low to medium stacking fault energy, DRX is marked and the characteristic stress–strain curves are observed to depend on the temperature, strain rate and initial grain size.[2,3)] Single–peak curves occur at a low temperature and high strain rate and multiple–peak curves occur at a high temperature and low strain rate. It is well–known that such characteristic mechanical behavior is strongly related to the microstructure evolution, or the nucleation and growth of DRX grains. Therefore, for the optimum design of the working process and the accurate prediction of material microstructures formed during hot working, it is essential to develop a numerical model that can be used to investigate the macroscopic mechanical behavior resulting from the microstructure evolution. However, since the modeling of DRX requires a simulation that couples the mechanical behaviors and the microstructure evolution, the number of reported numerical studies on DRX is much fewer than that for static recrystallization (SRX) occurring during post–deformation annealing.[4–11)]

The cellular automaton (CA) method[12–18)] and Monte Carlo (MC) method[19,20)] have been employed to simulate microstructure evolution during the DRX process. Because of its methodological flexibility, the CA method is used more frequently than the MC method. Ding and Guo[13)] developed a model that simulates the microstructural evolution and plastic flow behavior during DRX by coupling the evolution equation of dislocation density, or the Kocks-Meching (KM) model,[21)] with the CA method.[7)] Althought the DRX model is relatively simple and intuitive, it is possible to simulate the macroscopic mechanical behavior based on the microstructure. Therefore, the model is very useful as a multiscale method. However, it has been pointed out that the CA and MC methods lead to problems when modeling the absolute timescale and the curvature–driven growth of the grain boundary.[4)]

In this study, we develop a phase-field (PF) model to simulate microstructure evolution during DRX. Since the PF model can simulate the grain boundary migration by curvature driving with a real timescale, the grain growth is accurately reproduced.[22–29)] Here, the multi-phase-field (MPF) model proposed by Steinbach and Pezzolla[26)] is employed to represent polycrystalline material, because the MPF model has merits compared with other MPF models[27,28)] in that the phase field parameters can be perfectly related to the material parameters and the chemical driving force can be treated. Furthermore, the introduction of an algorithm developed by Kim *et al.*[29)] enables efficient MPF computation during DRX. Here, we call the developed model the multi-phase-field dynamic recrystallization (MPF-DRX) model. Subsequently, by performing a single–grain growth simulation, the accuracy of the MPF-DRX model is confirmed by comparison with theoretical results. Then, the results of polycrystalline grain growth are compared with those obtained by the CA method and we discuss the interrelationship between the microstructure and the mechanical behavior. Finally, the effects of the grain boundary mobility and nucleation rate on the DRX performance are investigated.

2. DRX Model

We develop the MPF-DRX model in which the grain growth driven by stored energy is simulated by the MPF method[26)] using an efficient computational algorithm[29)] and the dislocation density evolution due to plastic deformation and DRV is expressed by the KM model.[21)] A macroscopic

*Graduate Student, Kobe University

stress–strain curve is obtained from the Bailey–Hirsch relation[30] using the average dislocation density.

2.1 Multi-phase-field model

Let us consider a polycrystalline system including N grains. The αth grain is indicated by the phase field ϕ_α, where ϕ_α takes a value of 1 inside the αth grain, 0 inside the other grains and $0 < \phi_\alpha < 1$ at the grain boundary. The ϕ_α are not independent and must satisfy

$$\sum_{\alpha=1}^{N} \phi_\alpha = 1. \tag{1}$$

Here, we use the free energy functional

$$F = \int_V \Bigg[\sum_{\alpha=1}^{N} \sum_{\beta=\alpha+1}^{N} \Bigg(-\frac{a_{\alpha\beta}^2}{2} \nabla\phi_\alpha \cdot \nabla\phi_\beta + W_{\alpha\beta}\phi_\alpha\phi_\beta \Bigg) + f_\mathrm{e} \Bigg] dV, \tag{2}$$

where $a_{\alpha\beta}$ is the gradient coefficient, $W_{\alpha\beta}$ is the height of the energy barrier and f_e is the free energy density in the grains. Here, the number of grains, N, in eqs. (1) and (2) can be replaced with $n = \sum_{\alpha=1}^{N} \sigma_\alpha$, where $\sigma_\alpha = 1$ when $0 < \phi_\alpha \leq 1$ and 0 otherwise.

The evolution equation of the phase field ϕ_i is derived as[26]

$$\dot{\phi}_i = -\sum_{j=1}^{n} \frac{2M_{ij}^{\phi}}{n} \left(\frac{\delta F}{\delta \phi_i} - \frac{\delta F}{\delta \phi_j} \right), \tag{3}$$

where M_{ij}^{ϕ} is the phase field mobility. The functional derivative $\delta F/\delta\phi_i$ is calculated as

$$\frac{\delta F}{\delta \phi_i} = \sum_{k=1}^{n} \left(W_{ik}\phi_k + \frac{a_{ik}^2}{2} \nabla^2 \phi_k \right) + \frac{\partial f_\mathrm{e}}{\partial \phi_\mathrm{i}}. \tag{4}$$

Here, by selecting the driving term as $\partial f_e/\partial\phi_i - \partial f_e/\partial\phi_j = -\frac{8}{\pi}\sqrt{\phi_i\phi_j}\Delta E_{ij}$, where ΔE_{ij} is the difference in stored energy between grains i and j and $8/\pi$ is obtained from $\int_0^1 \sqrt{\phi_1\phi_2}d\phi = \int_0^1 \sqrt{\phi(1-\phi)}d\phi = \frac{\pi}{8}$, the evolution equation of the phase field ϕ_i reduces to

$$\dot{\phi}_i = -\sum_{j=1}^{n} \frac{2M_{ij}^{\phi}}{n} \Bigg[\sum_{k=1}^{n} \Bigg\{ (W_{ik} - W_{jk})\phi_k + \frac{1}{2}(a_{ik}^2 - a_{jk}^2)\nabla^2\phi_k \Bigg\} - \frac{8}{\pi}\sqrt{\phi_i\phi_j}\Delta E_{ij} \Bigg]. \tag{5}$$

Since the coefficients in eq. (5), a_{ij}, W_{ij} and M_{ij}^{ϕ}, are respectively related to the grain boundary thickness δ, grain boundary energy γ_{ij} and grain boundary mobility M_{ij} by

$$a_{ij} = \frac{2}{\pi}\sqrt{2\delta\gamma_{ij}}, \quad W_{ij} = \frac{4\gamma_{ij}}{\delta}, \quad M_{ij}^{\phi} = \frac{\pi^2}{8\delta} M_{ij}, \tag{6}$$

where the diagonal components are zero, the grain growth process can be reproduced quantitatively. For simplicity, it is assumed that all grain boundaries are high–angle grain boundaries with $\gamma_{ij} = \gamma$ and $M_{ij} = M$. Furthermore, the dislocation density is assumed to be constant in a grain. To calculate the driving force ΔE_{ij}, we introduce an additional variable ρ_i, defined in Fig. 1. Here, the variable ρ_i takes a constant dislocation density when $0 < \phi_i \leq 1$ and is zero when $\phi_i = 0$. The evolution of ρ_i follows the KM model expressed in the next section and ρ_i is updated after calculating phase field ϕ_i by eq. (5).

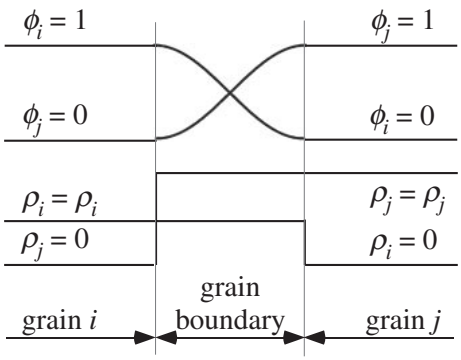

Fig. 1 Schematic illustration of profiles of phase fields and dislocation densities around grain boundary.

From a numerical point of view, the MPF model has a high computational cost, because usually N phase fields must be saved and N evolution equations must be solved at all grid points.[27,28] However, Steinbach and Pezzolla's MPF model has some computational merits. We do not have to solve eq. (5) at the grid points with $n = 1$ and it is sufficient to save not N but n phase fields at a grid point. To further improve the computational efficiency, we introduce the algorithm proposed by Kim *et al.*[29] and modify it to achieve more accurate computation. The procedure is as follows:

(1) Solve eq. (5) for n phase fields.
(2) During (1), if ϕ_i at the previous time step is zero and the calculated increment $\Delta\phi_i$ has a negative value, phase field ϕ_i is removed from the phase field group that must be solved at the grid point and we set n to $n-1$.
(3) Steps (1) and (2) are repeated until all phase fields satisfying the above condition are removed.
(4) The n phase fields are rearranged in order of decreasing size. Phase fields from the largest to n_ϕth largest are recorded. Here, n_ϕ is a predefined maximum number of the recorded phase field.
(5) The phase fields are replaced by $\phi_i^* = \phi_i / \sum_{j=1}^{n_\phi} \phi_j$. so as to satisfy $\sum_{i=1}^{n_\phi} \phi_i^* = 1$.
(6) If a phase field is not saved at grid point (l, m) and its value at grid points $(l \pm 1, m \pm 1)$, or the nearest four neighbors, is not zero, the phase field is added to the phase field group at the grid point (l, m). Therefore, the number of phase fields solved in step (1) sometimes becomes more than n_ϕ.

Steps (1) to (6) are repeated in each time step.

2.2 Dislocation evolution model

The accumulation of dislocations due to plastic deformation and DRV is expressed by the KM model[21] as a relationship between dislocation density and true strain,

$$\frac{d\rho}{d\varepsilon} = k_1\sqrt{\rho} - k_2\rho. \tag{7}$$

Here, the first term of the right–hand side expresses the work hardening, where k_1 is a constant that represents hardening. The second term is the DRV term, where k_2 is a function of

temperature T and strain rate $\dot{\varepsilon}$.[13] The macroscopic stress is related to the average dislocation density $\bar{\rho}$ as follows:

$$\sigma = \alpha\mu b\sqrt{\bar{\rho}}, \tag{8}$$

where α is a dislocation interaction coefficient of approximately 0.5, μ is the shear modulus and b is the magnitude of the Burgers vector. From eqs. (7) and (8), a macroscopic stress–strain curve can be determined.

2.3 Computational procedure

The computational procedure of the developed MPF-DRX model is as follows:

(1) The initial polycrystalline structure is created by a conventional grain growth simulation.
(2) The dislocation density at all grid points is set to the initial value ρ_{ini}.
(3) The dislocation density and macroscopic stress–strain curve up to the DRX nucleation point are calculated under a constant strain increment $\Delta\varepsilon = \dot{\varepsilon}\Delta t$ by eqs. (7) and (8), where Δt is the time increment.
(4) If the dislocation density on a grain boundary exceeds the critical value ρ_c required to create a nucleus, a circular nucleus with dislocation density ρ_{ini} is placed on the grain boundary with nucleation rate $\dot{n}$.
(5) The DRX grain growth is simulated by solving eq. (5).
(6) The dislocation density variables at all grid points and the macroscopic stress are calculated by eqs. (7) and (8).

Steps (4) to (6) are repeated until a predefined strain value is reached.

3. Numerical Conditions

By performing numerical simulations using the MPF-DRX model, first, we confirm the accuracy of the developed model, second, we compare the results of the MPF-DRX simulation with those of the CA simulation by Kugler and Turk[16] and, finally, we evaluate the effects of the grain boundary mobility and nucleation rate on the DRX process. A series of simulations are performed for copper at temparature $T = 800\,\mathrm{K}$ and strain rate $\dot{\varepsilon} = 0.002\,\mathrm{s}^{-1}$.

The material and numerical parameters used in the following simulations are as follows: For eqs. (5) and (6), grid space $\Delta x = 0.5\,\mu\mathrm{m}$, grain boundary energy $\gamma = 0.208\,\mathrm{J/m^2}$, grain boundary thickness $\delta = 7\Delta x$ and grain boundary mobility $M = M_0/T\exp(-Q_b/RT)$, where $M_0 = 0.139\,\mathrm{m^4\,K/Js}$, the activation energy $Q_b = 110\,\mathrm{KJ/mol}$ and R is the gas constant. For eqs. (7) and (8), $k_1 = 4.00 \times 10^8/\mathrm{m}$ and $k_2 = \alpha\mu b k_1/\sigma_{st}$, where $\alpha = 0.5$, shear modulus $\mu = 42.1\,\mathrm{GPa}$, the magnitude of the Burgers vector $b = 2.56 \times 10^{-10}\,\mathrm{m}$ and the steady-state stress $\sigma_{st} = \{A_1\dot{\varepsilon}\exp(Q_a/RT)\}^{1/A_2}$, where $A_1 = 2.0 \times 10^{44}$, $A_2 = 7.6$ and activation energy $Q_a = 275\,\mathrm{KJ/mol}$. For DRX nucleation, we set the critical stress σ_c to 40 MPa, which corresponds to the critical dislocation density $\rho_c = (\sigma_c/\alpha\mu b)^2 = 5.51 \times 10^{13}/\mathrm{m^2}$, and we employ the nucleation rate per unit area of the grain boundary expressed by $\dot{n} = c\dot{\varepsilon}^d\exp(-Q_a/RT)$,[13] where $c = 5.0 \times 10^{25}$ and $d = 1$. Here, one nucleus is created every $(\dot{n}\Delta t n_{gb}\Delta x^2/\delta)^{-1}$ steps, where n_{gb} is the number of grid points located in the grain boundary or satisfying $0 < \phi_i < 1$. The initial dislocation density is set to $\rho_{ini} = 10^9/\mathrm{m^2}$, the time increment $\Delta t = 0.013\,\mathrm{s}$ and the predefined maximum number of the recorded phase field $n_\phi = 5$.

For comparison with the CA simulation, we mostly employed the parameters used in Ref. 16) as shown above. However, some points are different. The first difference is that we use a grain boundary energy that is one–third of the value given in Ref. 16), $0.625\,\mathrm{J/m^2}$. If we use $\gamma = 0.625\,\mathrm{J/m^2}$, the nucleus diameter sufficiently overcomes the curvature energy and becomes over 15 μm, which is too large. In Refs. 13) and 16), the cell size is set to 2 μm and one cell is used as one nucleus. Since the PF method can model the curvature effect accurately, such a small nucleus shrinks and disappears. Therefore, to reduce the nucleus diameter, we set $\gamma = 0.208\,\mathrm{J/m^2}$. This is a fitting parameter determined so as to include the effects of real nucleation mechanism. It has been reported that actual DRX nucleation occurs through processes such as grain boundary migration, grain boundary serration, grain boundary sliding and twin nucleation[31–34] and, to simulate the nucleation process with high accuracy, homogeneous plastic deformation and DRX grain growth must be simulated simultaneously and further study is necessary. The second difference is the nucleation condition. Since the critical dislocation density ρ_c and nucleation rate $\dot{n}$ are not given explicitly in Ref. 16), we employed the nucleation rate model proposed by Ding and Guo[13] and the coefficients c and d are determined so as to obtain almost the same steady-state grain size D_s as that shown in Fig. 4 in Ref. 16). Final difference is the value of k_1 in eq. (7). We selected its value so that the stress–strain curve calculated from eqs. (7) and (8) can be fit to the curve shown in Fig. 4(a) of Ref. 16).

4. Numerical Results

4.1 Single–grain growth simulation

To confirm the validity of the developed MPF-DRX model, a single–grain growth simulation is performed and the variations in the migration rate of the grain boundary are compared to theoretical results. Here, we use a square computational domain of $50 \times 50\,\mu\mathrm{m}$ (100×100 lattice) with a zero Neumann boundary condition on all sides. A circular nucleus of radius 2.74 μm is placed at the grid point $(l, m) = (1, 1)$. The initial dislocation densities in the nucleus ρ_r and the deformed material ρ_m are set to $\rho_r = \rho_{ini}$ and $\rho_r = \rho_c$, respectively.

Figure 2(a) shows the variations in the grain boundary migration rate V obtained from the PF simulation and the theoretical equation, $V_{th} = M(\Delta E - \gamma/r)$, where r is the radius of the DRX grain. From Fig. 2(a), the result of the PF simulation agrees well with the theoretical results and, therefore, it is verified that the developed PF model can simulate the DRX growth process accurately. For comparison, the result of SRX with constant driving force $\Delta E = 0.09\,\mathrm{MPa}$ is also shown in Fig. 2(a). In the case of SRX, since the driving force is constant, the migration rate of the grain boundary increases monotonically with increasing SRX grain size. On the other hand, in the case of DRX, the dislocation densities inside both the DRX grain ρ_r and the deformed grain ρ_m change with strain. Furthermore, the rate

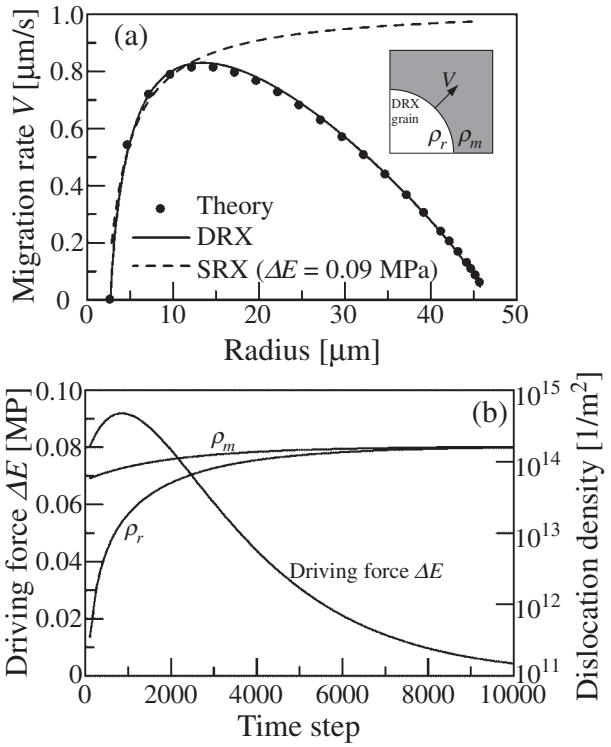

Fig. 2 Variations in (a) migration rate of grain boundary and (b) driving force ΔE and dislocation densities in DRX grain ρ_r and deformed material ρ_m.

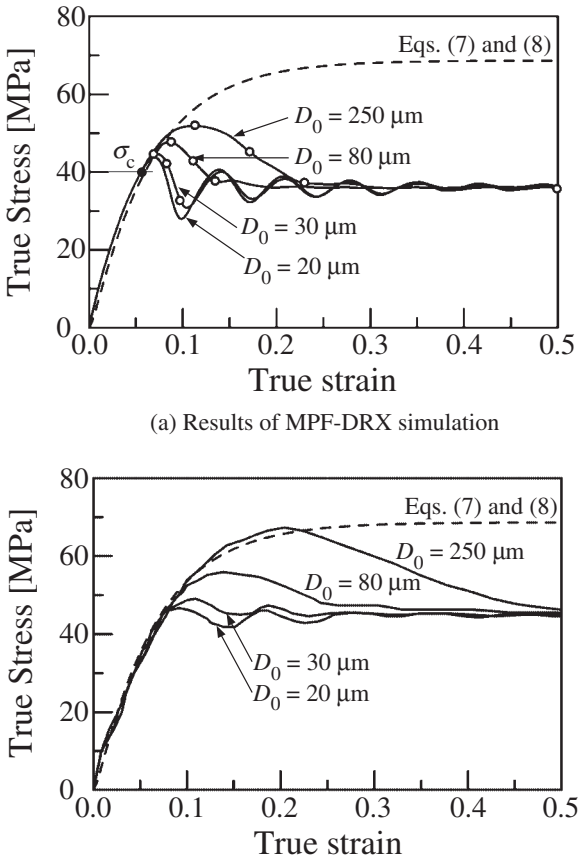

(a) Results of MPF-DRX simulation

(b) Results of CA simulation by Kugler and Turk[16)]

Fig. 3 Macroscopic stress–strain curves.

of increase of dislocation density is greater in the DRX grain than in the deformed grain, as shown in Fig. 2(b). As a result, depending on the driving force balance between the stored energy and the curvature, the grain boundary migration rate exhibits the characteristic change shown in Fig. 2(a).

4.2 DRX microstructure evolution

Macroscopic stress–strain curves and the microstructural evolution during the DRX process for the polycrystalline material are simulated by the MPF–DRX model by changing the initial grain size D_0 and are compared with those obtained by the CA simulation reported by Kugler and Turk.[16)] Initial polycrystalline structures with grain size $D_0 = 20$, 30, 80 and 250 μm are prepared using conventional grain growth simulations. The initial grain shape is set to be a regular hexagon. Computational domain sizes of 532.5 × 527.0 μm (1065 × 1054 lattice), 513.5 × 543.0 μm (1027 × 1086 lattice), 532.5 × 527.0 μm (1065 × 1054 lattice) and 476.5 × 412.5 μm (953 × 825 lattice) are employed and the numbers of initial grains are 896, 396, 56 and 4 for $D_0 = 20$, 30, 80 and 250 μm, respectively.

Figures 3 and 4 show the macroscopic stress–strain curves and variations in average grain size, respectively. The dashed line in Fig. 3 is the stress–strain curve calculated by eqs. (7) and (8), i.e., without DRX. Figures 3(b) and 4(b) show the results shown in Fig. 4 in Ref. 16). Comparing Figs. 4(a) with 4(b), the strain at which the decrease in average grain size starts and the steady–state grain size D_s are observed to be almost identical, because the critical stress σ_c necessary to create the DRX nucleus and the nucleation rate $\dot{n}$ are determined so that these values become equal. However, we can see some differences in the rate of variation of average grain size during DRX. The differences between the present results and those obtained by the CA simulation can be observed more clearly in Fig. 3. Although similar changes in the stress–strain curve are observed in Figs. 3(a) and 3(b), we can see remarkable differences in the peak stress. Because, as shown in the previous section, our MPF model can simulate the DRX growth process accurately, it is thought that the differences originate from the time scaling method used in the CA model.

Next, we discuss the effects of the initial grain size D_0 on the DRX process. Figure 5 shows the microstructural evolution for $D_0 = 30$, 80 and 250 μm. The gray grains indicate the initial grains and the white grains are the DRX grains. The strain values in Fig. 5 correspond to the open circles in Fig. 3(a). For $D_0 = 30$ μm, perfectly random nucleation and growth are observed and for $D_0 = 250$ μm, typical necklace structures are formed.[1)] However, the steady–state microstructures at $\varepsilon = 0.500$ exhibit an equi-axed grain structure without initial grain size dependence. Although the nucleation rate per unit area of the grain boundary is constant, the grain boundary area increases with decreasing initial grain size D_0. As a result, the peak stresses of the stress–strain curves shown in Fig. 3 decrease as D_0 becomes small. Futhermore, for small D_0, the stress–strain curves have multiple peaks, while single–peak curves are observed for large D_0. It is known that the transition from single to multiple peaks depends on whether or not the

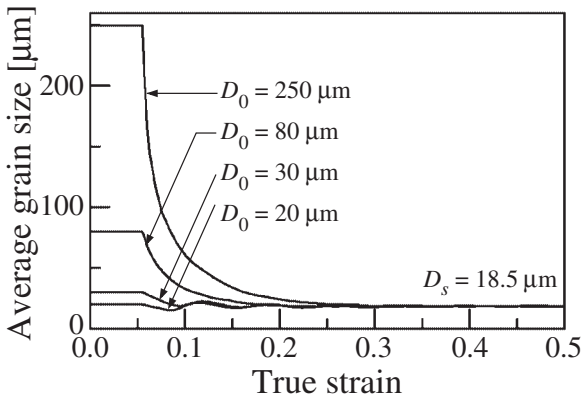

(a) Results of MPF-DRX simulation

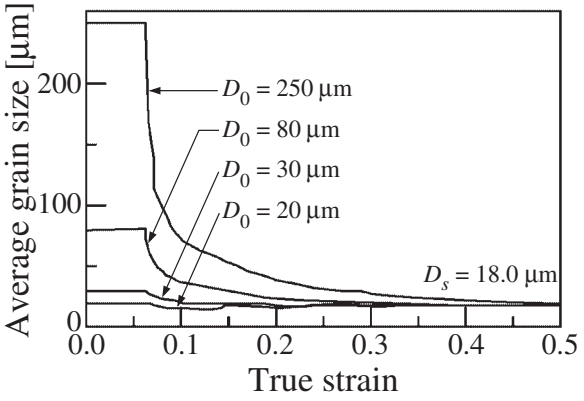

(b) Results of CA simulation by Kugler and Turk[16)]

Fig. 4 Variations in average grain size.

recrystallization cycles overlap.[2)] In Fig. 5, three microstructures from the first peak stress to the first valley stress and the steady–state microstructure are illustrated. In the case of $D_0 = 30\,\mu\text{m}$, the DRX nuclei in secondary cycle are created after the first DRX cycle is completed. On the other hand, for $D_0 = 80$ and $250\,\mu\text{m}$, the secondary DRX cycle has started already when $\varepsilon = 0.136$ and 0.172, respectively, while initial grains are still remain. These phenomena agree well with the experimental and numerical results reported so far.[1,2,13,16,35)] From these results and the discussion, it is confirmed that the proposed MPF–DRX model can simulate the macroscopic mechanical behavior based on the microstructure evolution with high accuracy.

4.3 Effects of mobility and nucleation rate

Since the DRX model employed in this study assumes that the dislocation density inside a grain is constant, the nucleation criteria and the determination of some parameters, such as k_1, k_2, A_1, A_2, c, d and M, are thought to be important. Therefore, we discuss the effects of the grain boundary mobility M and nucleation rate $\dot{n}$ on DRX.

Figures 6 and 7 show (a) macroscopic stress–strain curves, (b) variations of the average grain size and (c) variations of the number of grains calculated by changing M and c, respectively. The values of grain boundary mobility M are changed to $0.25M_s$, $0.50M_s$, $1.00M_s$ and $2.00M_s$, where M_s is the grain boundary mobility used in sections 4.1 and 4.2. From Fig. 6(a), the peak stress increases with decreasing M

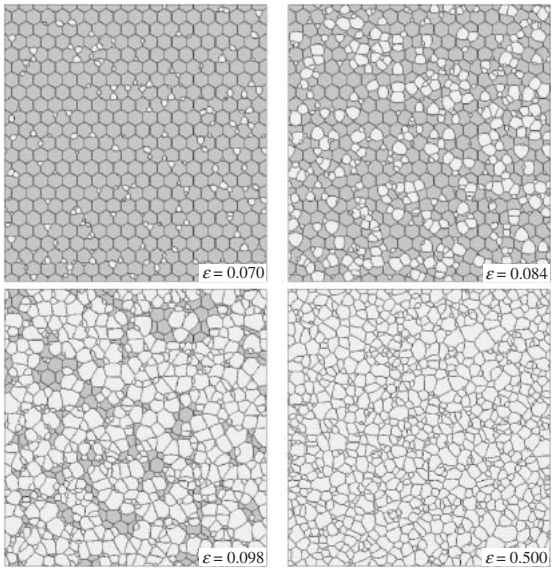

(a) $D_0 = 30\ \mu\text{m}$

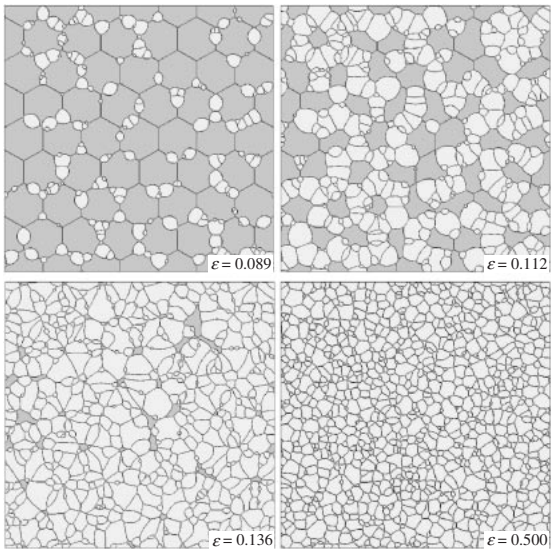

(b) $D_0 = 80\ \mu\text{m}$

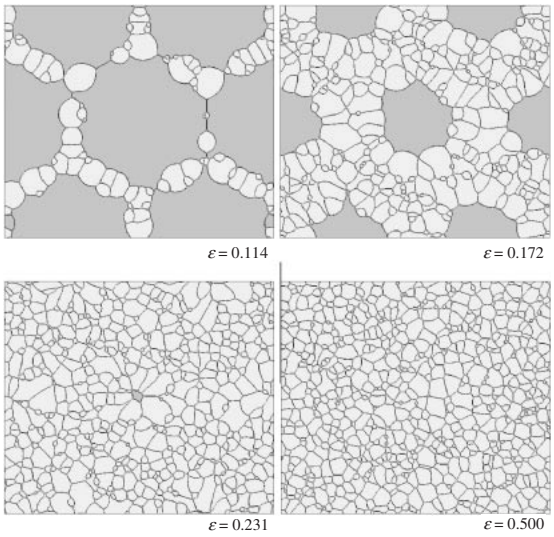

(c) $D_0 = 250\ \mu\text{m}$

Fig. 5 Microstructure evolution. The gray grains are initial grains and the white grains are DRX grains. The strain values correspond to the open circles in Fig. 3(b).

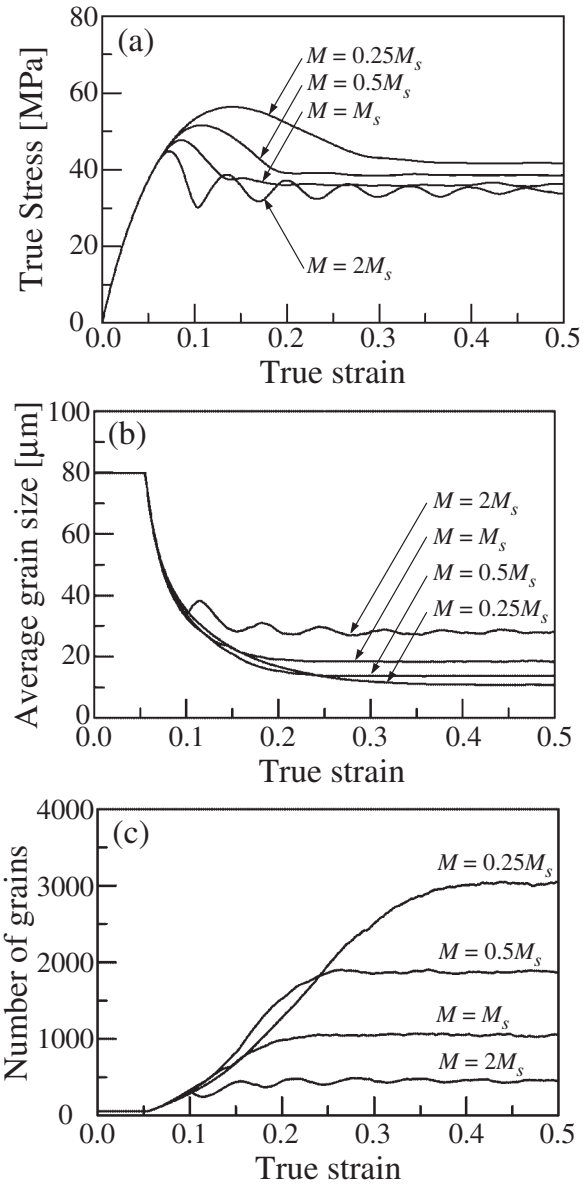

Fig. 6 Effects of grain boundary mobility on (a) stress-strain curve, (b) average grain size and (c) number of grains.

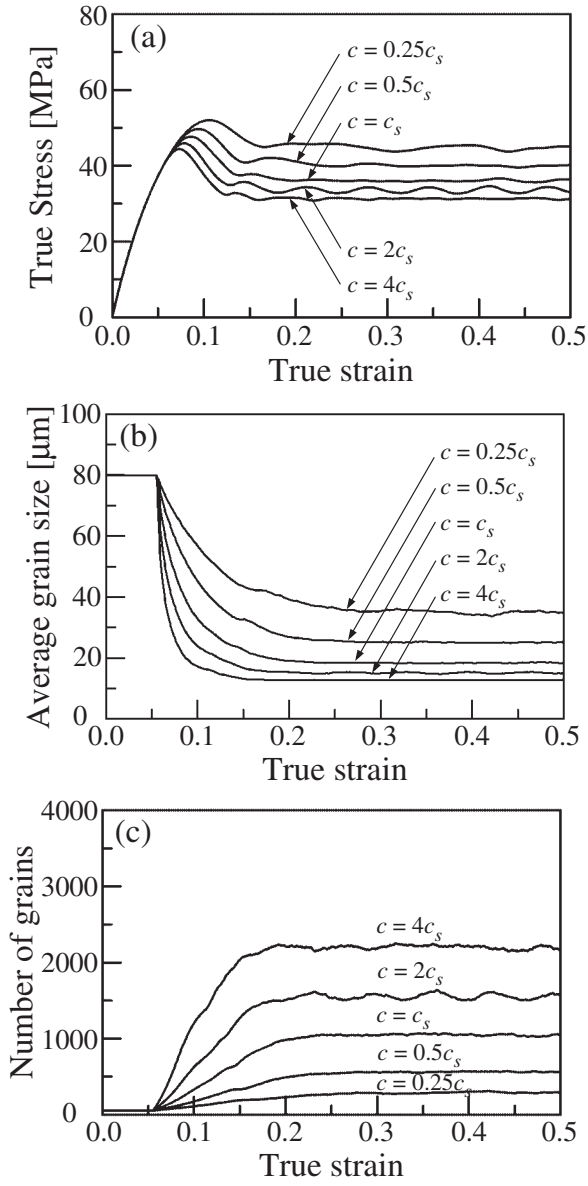

Fig. 7 Effects of nucleation rate on (a) stress-strain curve, (b) average grain size and (c) number of grains.

and multiple peaks can be observed for $M = 2M_s$. These are similar characteristics to those in Fig. 3(a) or obtained when changing the initial grain size D_0. However, the steady–state stresses are not the same value in Fig. 6(a). Also, the grain size does not converge to the same value, as shown in Fig. 6(b). The effect of the nucleation rate is evaluated by changing c to $0.25c_s$, $0.50c_s$, $1.00c_s$, $2.00c_s$ and $4.00c_s$, where c_s is the value used in section 4.2. As can be seen in Figs. 7(a) and 7(b), the peak stress, steady–state stress and steady–state grain size increase with decreasing c or nucleation rate $\dot{n}$. Furthermore, the stress–strain relationships all have single–peak curve and never exhibit multiple peaks. As discussed here, by changing only the grain boundary mobility or the nucleation rate, we cannot simultaneously reproduce the transition from single to multiple peaks in the stress–strain curves and the constant steady-state grain size observed when changing the initial grain size. Therefore, it can be concluded that the balance between the grain growth rate and the nucleation criteria of DRX is important in expressing actual DRX phenomena. Furthermore, from Figs. 6(c) and 7(b), we can see that many phase field variables are used during DRX simulations, particularly for a small grain boundary mobility and large nucleation rate, because one grain is expressed by one phase field. Therefore, it is confirmed that efficient computation can be achieved by introducing the algorithm used for the MPF method.

5. Conclusions

We have developed the MPF-DRX model to accurately simulate the microstructure evolution and macroscopic mechanical behavior during hot working. An efficient numerical simulation was achieved by introducing an efficient computational algorithm for the MPF method. The accuracy of the developed MPF method was confirmed by comparing the grain boundary migration rate of single–grain

growth with that predicted from the theoretical equation. By performing DRX simulations under almost same conditions as that used in a previously reported CA simulation, we compared the results obtained by the MPF and CA methods. As a result, we observed a difference in the recrystallization kinetics. Furthermore, by investigating the effects of the initial grain size on DRX, it was confirmed that some phenomena observed in the experiment, such as the transition from single to multiple peaks in the macroscopic stress–strain curve and the independence of steady–state average grain size on the initial grain size, can be simulated. Also, the interrelationship between the microstructure evolution and the macroscopic mechanical behavior was discussed. Finally, the effects of the grain boundary mobility and DRX nucleation rate were evaluated by changing each parameter. It was concluded that the balance between the grain growth rate and the nucleation criteria of DRX is important in expressing actual DRX phenomena.

As a next step to the present study, the development of a method for determining some of the parameters is important, because the plastic deformation is expressed by the simple equation of dislocation density evolution. In a future study, we hope to develop a coupling model that enables the simultaneous evaluation of plastic deformation and DRX grain growth.

Acknowledgements

This research was partially supported by a Ministry of Education, Culture, Sports, Science and Technology Grant-in-Aid for Scientific Research and the Japan Aluminium Association. We also gratefully acknowledge helpful discussions with Dr. Yoshihiro Suwa on the MPF method and the related computation.

REFERENCES

1) F. J. Humphreys and M. Hatherly: *Recrystallization and Related Annealing Phenomena*, (Elsevier, 2004) pp. 415–450.
2) T. Sakai and J. J. Jonas: Acta Metall. **32** (1984) 189–209.
3) W. Roberts and B. Ahlblom: Acta Metall. **26** (1978) 801–813.
4) M. A. Miodownik: J. Light Metals **2** (2002) 125–135.
5) D. J. Srolovitz, G. S. Grest and M. P. Anderson: Acta Metall. **34** (1986) 1833–1845.
6) B. Radhakrishnan, G. B. Sarma and T. Zacharia: Acta Mater. **46** (1998) 4415–4433.
7) H. W. Hesselbarth and I. R. Gobel: Acta Metall. Mater. **39** (1991) 2135–2143.
8) V. Marx, R. R. Reher and G. Gottstein: Acta Mater. **47** (1999) 1219–1230.
9) D. Raabe and R. C. Becker: Model. Sim. Mater. Sci. Eng. **8** (2000) 445–462.
10) Y. Suwa, Y. Saito and H. Onodera: Mater. Sci. Eng. A **457** (2007) 132–138.
11) T. Takaki, A. Yamanaka, Y. Higa and Y. Tomita: Sci. Model. Sim. **14** (2007) 75–84.
12) R. L. Goetz and V. Seetharaman: Scr. Mater. **38** (1998) 405–413.
13) R. Ding and Z. X. Guo: Acta Mater. **49** (2001) 3163–3175.
14) R. Ding and Z. X. Guo: Mater. Sci. Eng. A **365** (2004) 172–179.
15) M. Qian and Z. X. Guo: Mater. Sci. Eng. A **365** (2004) 180–185.
16) G. Kugler and R. Turk: Acta Mater. **52** (2004) 4659–4668.
17) R. L. Goetz: Scr. Mater. **52** (2005) 851–856.
18) N. Xiao, C. Zheng, D. Li and Y. Li: Comp. Mater. Sci. **41** (2008) 366–374.
19) A. D. Rollett, M. J. Luton and D. J. Srolovitz: Acta metall. Mater. **40** (1992) 43–55.
20) P. Peczak: Acta Metall. Mater. **43** (1995) 1279–1291.
21) H. Mecking and U. F. Kocks: Acta Metall. **29** (1981) 1865–1875.
22) R. Kobayashi: Physica D **63** (1993) 410–423.
23) J. A. Warren and W. J. Boettingera: Acta Metall. Mater. **43** (1995) 689–703.
24) A. Yamanaka, T. Takaki and Y. Tomita: Mate. Trans. **47** (2006) 2725–2731.
25) T. Takaki, T. Fukuoka and Y. Tomita: J. Crystal Growth **283** (2005) 263–278.
26) I. Steinbach and F. Pezzolla: Physica D **134** (1999) 385–393.
27) L.-Q. Chen and W. Yang: Phys. Rev. B **50** (1994) 15752–15756.
28) D. Fan and L.-Q. Chen: Acta Mater. **45** (1997) 611–622.
29) S. G. Kim, D. I. Kim, W. T. Kim and Y. B. Park: Phys. Rev. E **74** (2006) 061605.
30) J. E. Bailey and P. B. Hirsch: Philos. Mag. **5** (1960) 485–497.
31) A. M. Wusatowska-Sarnek, H. Miura and T. Sakai: Mater. Sci. Eng. A **323** (2002) 177–186.
32) H. Miura, T. Sakai, R. Mogawa and G. Gottstein: Scr. Mater. **51** (2004) 671–675.
33) H. Miura, T. Sakai, S. Andiarwanto and J. J. Jonas: Philos. Mag. **85** (2005) 2653–2669.
34) H. Miura, T. Sakai, R. Mogawa and J. J. Jonas: Philos. Mag. **87** (2007) 4197–4209.
35) L. Blaz, T. Sakai and J. J. Jonas: Metal Sci. **17** (1983) 609–616.